2007 IEEE International Conference on
Robotics and Automation
Roma, Italy, 10-14 April 2007

Control of Harmonic Drive Motor Actuated Flexible Linkages

J.-P. Hauschild and G. R. Heppler

Abstract— **Friction models and compensation methods are applied to harmonic drive motors used with flexible robotic linkages. In the absence of output torque measurements and output shaft encoder data nearly complete friction compensation is achieved allowing the application of a passivity based controller. Simulation and experimental results are given.**

I. INTRODUCTION

Because of the absence of backlash and high gear ratios servo-actuators with harmonic drive gearing are commonly used for space manipulators. One of their major drawbacks is the high level of internal friction in the transmission and the difficulties this gives rise to with regard to controller design and implementation. In addition to the friction caused by the DC-motor brushes and the bearings, the harmonic drive gearing in the actuators causes a major part of the total friction due to the flex-spline and the large gear tooth area. The friction is nonlinear and is dependent on the state of the motor and its environment. In the sequel we investigate the friction behavior of harmonic drive (HD) actuators, present friction compensation methods that reduce the level of apparent friction and illustrate how the friction compensation allows application of a passivity based controller to a HD actuated flexible link robotic linkage.

II. FRICTION MODELS

A wide range of friction models have been thoroughly reviewed by Armstrong-Hélouvry *et al.*[1] and Olsson *et al.*[2]. The Coulomb friction model and its extensions have difficulties when the velocity is near zero because of the jump discontinuity in that region. A more general model of friction is

$$F = \begin{cases} F(v) & \text{if } v \neq 0 \\ F_e & \text{if } v = 0 \text{ and } |F_e| < F_S \\ F_S\, sgn(F_e) & \text{otherwise} \end{cases} \quad (1)$$

where $F(v)$ is an arbitrary function often chosen to be

$$F(v) = \left(\alpha_0 + \alpha_1 \exp\left(-(v/v_S)^{\delta}\right)\right) sgn(v) + \alpha_2 v \quad (2)$$

It covers Coulomb, viscous, static and Stribeck [3] friction and is characterized by the parameters: $\alpha_0 = F_C$ (Coulomb friction), $\alpha_1 = F_S - F_C$ (additional stiction force), $\alpha_2 = F_v$ (viscous friction coefficient), v_S (Stribeck velocity), and the form factor δ, with different parameters used for opposite directions. A disadvantage of model (1) is the problem of detecting when the velocity is zero. Model (1) and (2) will be referred to as the exponential friction model.

The Lund-Grenoble (LuGre) model [4] combines stiction and the Dahl effect [5] with steady state friction characteristics like Coulomb friction, viscous friction and the Stribeck effect. It uses an internal state variable z governed by

$$\dot{z} = v - (\sigma_0/g(v))|v|z \quad (3)$$

where v is the relative velocity between the two surfaces, and σ_0 is the stiffness parameter. The function $g(v)$ is positive and depends on factors like lubrication, material properties, and temperature. To recover the Stribeck effect it decreases monotonically as v increases. It is proposed [4] that

$$g(v) = \alpha_0 + \alpha_1 \exp\left((-v/v_S)^2\right) \quad (4)$$

The corresponding friction force is described by

$$F = \sigma_0 z + \sigma_1 \dot{z} + \alpha_2 v \quad (5)$$

where the first two terms denote the force generated by surface interactions and the last term is the viscous friction.

III. FRICTION COMPENSATION

Friction compensation methods to be discussed here are restricted to those applicable to HD actuators without output torque measurements or output shaft encoders. The simplest way to compensate friction in servo drives is a feed-forward element as shown in Fig. 1 (with the feedback part removed). A friction torque $\tau_f(\tau)$ is added to the input torque τ as an offset to the input signal for the motor depending on the sign of the input. In the ideal case, this offset should be exactly the friction torque but in practice the offset should always under compensate the real friction to avoid instabilities. Feed-forward compensation is limited to the reduction of the Coulomb friction. It cannot compensate stiction effects nor viscous friction, does not provide back drivability to the motor, would not prevent large steady state errors and it would increase the non-linearities of the motor [6].

Compensation based on Coulomb friction based models has an infinite slope for a zero input which can cause an undesirable chattering when the friction compensation is used in a direct feedback loop. A remedy would be a decreased slope at zero input [7], but the steady-state error of the system can still increase due to the under compensation of the friction at low velocities.

An extension of the feed-forward friction compensation is shown in Fig. 1 where there is now an additional feedback element which provides a compensation for viscous friction and can include the Stribeck effect. A compensation of the stiction force is theoretically possible, but in practice not

J.-P. Hauschild is with Electrical Engineering, Technical University of Hamburg-Harburg, 21073 Hamburg, Germany jp.hauschild@tu-harburg.de

G. R. Heppler is with the Department of Systems Design Engineering, University of Waterloo, Waterloo, ON N2L 3G1, Canada heppler@uwaterloo.ca

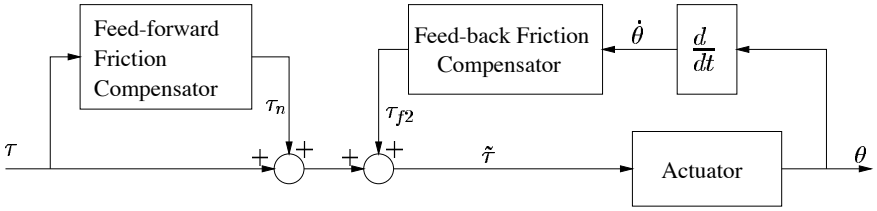

Fig. 1. Combination of feed-forward and feedback friction compensation.

applicable because an infinite slope of both compensators for zero velocity would cause chattering. Reducing this slope would result in a zero velocity reading and therefore prevent any feedback compensation. This type of friction compensation introduces an increased nonlinearity as in the pure feed-forward case. Many friction compensators use velocity feedback similar to that shown in Fig. 1 (but without the feed-forward element) to estimate a friction torque and add it to the input signal. This configuration has one major drawback: the starting of the motor from rest needs an input torque which is higher than the stiction torque of the motor. This torque should be provided by the friction model, but the friction model will not be in effect until the motor is moving. This behavior is especially of interest for actuators with harmonic drive gearing because the ratio between the stiction torque and rated output torque is quite high (about $1/5$ for the HD actuators used here). For control purposes, the actual working torques are often far below the rated output torques and get close to zero when reaching the control objective. For these reasons, a modification to the friction compensation scheme is required.

A modified velocity feedback scheme, or *modified friction compensation*, that mitigates the drawbacks of pure velocity feedback is shown in Fig. 2. Velocity feedback is preserved, but the velocity signal is modified, based on the current input signal, near zero.

Cross-fading between the velocity and the input signal is used to allow inclusion of the current motor speed with the input signal to estimate the friction torque for velocities near zero (Fig. 2). The modified signal $\tilde{\theta}$ is then used for the

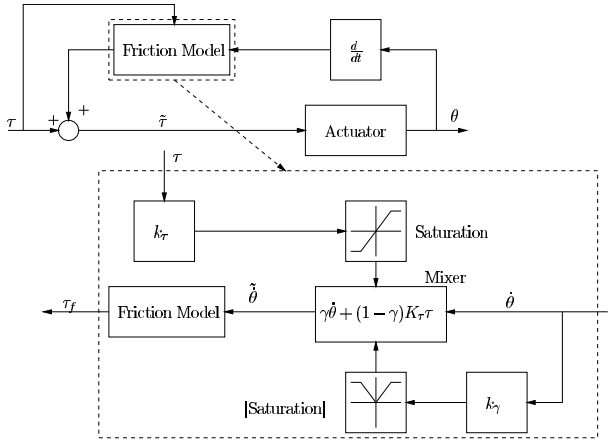

Fig. 2. Modified velocity feedback scheme.

friction compensation. The saturation of the input signal $\tau \in [-\delta, \delta]$ guarantees that the modified velocity $\tilde{\theta}$ never causes a friction model output τ_f larger than the real friction torque. The mixing ratio γ is generated by an amplified and saturated velocity $\dot{\theta}$ as per:

$$\gamma = \begin{cases} k_\gamma|\dot{\theta}| & \text{for } k_\gamma|\dot{\theta}| < 1 \\ 1 & \text{for } k_\gamma|\dot{\theta}| \geq 1 \end{cases} \tag{6}$$

The speed at which the friction model is fully based on the real velocity is set with the factor k_γ; the gain k_τ takes care of the conversion from input torque to pseudo-speed $\dot{\theta}_\tau$. The mixing of the two signals is linear as shown. The modified friction compensation is capable of covering all the friction phenomena that the pure velocity feedback configuration does and it is also able to compensate for input signals with smaller magnitude than the stiction force.

IV. EXPERIMENTS AND RESULTS

The experiments reported here were conducted on a HD Systems RFS-32-6030 motor rated at 50 Nm output torque with a $50:1$ HD gear box, a mass of 11.8 kg and moment of inertia $J = 3.41$ kgm^2. Similar experiments, with similar results, were also conducted on an HD Systems RFS-25-6018 motor (30 Nm output torque, $50:1$ gearing) [6].

The joint angle was measured with an optical encoder that had a physical resolution of 1024 pulses per revolution, a quadrature decoder that gave a resolution multiple of four, and a gear ratio multiple of 50. The overall resolution was 204800 pulses per revolution.

The friction was qualitatively observed to depend on the absolute motor angle and temperature. The friction compensated motor was to behave like an ideal motor (including back drivability) with a transfer function $G(s) = 1/(Js^2)$ so that: model based linear controllers could be used, it could handle small input signals (the desired output torque might be smaller than the break-out torque), there was no chattering, and it would be possible to apply the friction compensation to different control algorithms without changes. To fulfill these requirements the LuGre model was chosen from several different friction models and compensation schemes [6], [8].

A. Friction Compensation with the LuGre Model

A HD-motor with friction was modelled using (3)–(5) and

$$J\ddot{\theta} = \tau - \tau_f \tag{7}$$

where θ is the angular position of the motor, $\dot{\theta} = v$ from (3) is the angular velocity, $\tau_f = F$ from (5) is the friction torque

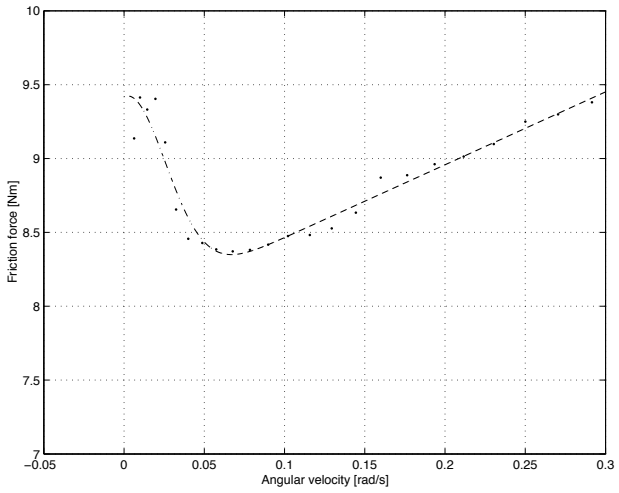

Fig. 3. Static friction–velocity map (•; measurement; –:parameterization).

and τ is the torque of the ideal motor. The static parameters of the LuGre model α_0, α_1, α_2, and v_S from (4) can be estimated by constructing a friction–velocity map measured during constant velocity rotation. The friction torque was measured in a closed loop experiment under velocity PI control[6]. The dynamic parameters σ_0 and σ_1 were then determined using the static parameter values and open-loop experiments that included zero crossings of the velocity were performed. The recorded data was used to search for a $\hat{\sigma} = [\hat{\sigma_0}, \hat{\sigma_1}]$ that minimized the error cost function

$$E\{\theta, \theta_m; \hat{\sigma}\} = \sum_{k=0}^{N} [\theta(k, \sigma) - \theta_m(k, \hat{\sigma})]^2 \qquad (8)$$

where $\theta(k, \sigma)$ is the k^{th} sampled actuator angle and $\theta_m(k, \hat{\sigma})$ is the k^{th}-value of the model output position.

Because of the temperature dependency of the harmonic drive, the experiment scanned the speed range 0.0004 rad/s to 0.61 rad/s in one test[6]. Each desired speed was allowed to settle into steady-state motion and then averages of all input torque and output speed values were calculated. The resulting static friction–velocity map is shown as dots in Fig. 3. The higher density of data points at low speeds is evident in this figure. Only the positive direction is shown here but similar results were obtained for the negative direction. Different parameter sets for each direction were determined for the steady-state friction torque by using a non-linear optimization multi-variable simplex search. Results are shown with a dashed line in Fig. 3. The resulting steady-state parameters are given in Table I.

To find values for the two dynamic parameters σ_0 and σ_1 open-loop experiments that included zero velocity crossings

TABLE I

PARAMETERS OF THE LUGRE MODEL.

Parameter	Value for positive part	Value for negative part
α_0	7.9707 Nm	7.7538 Nm
α_1	1.4476 Nm	0.8626 Nm
α_2	4.9349 Nms/rad	4.3267 Nms/rad
v_S	0.0363 rad/s	0.0221 rad/s
σ_0	259 Nm/rad	259 Nm/rad
σ_1	10 Nms/rad	10 Nms/rad

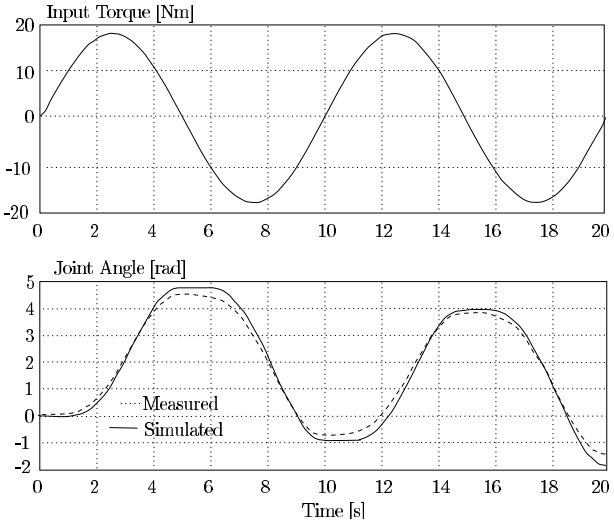

Fig. 4. Dynamic parameter estimation: real and simulated angle.

were performed. It was found that the values given in Table I gave good agreement between the simulated and the real actuator response as shown in Fig. 4. The validation of the LuGre friction model with the determined parameters was performed under friction compensation. If friction can be exactly predicted the actuator under friction compensation would behave like an ideal motor with no energy dissipation. In a P-controlled closed loop experiment, an ideal system would behave as an oscillator without friction. Therefore, small imprecisions in the friction model would lead either to decay if friction is under estimated or to an unstable behavior if friction is over estimated.

The experimental setup was implemented according to the modified friction compensation configuration (Fig. 2) with the following parameters: $k_\gamma = 100$ s, $k_\tau = 1$ rad/Nms, $\delta = \pm 0.5$ s^{-1}. The controller for the validation setup had a P-gain of 5 Nm, and the step input at 1 s had a magnitude of 1 rad. The step response of the friction compensated system is shown in Fig. 5 as a solid line; additionally a dashed line shows the simulated step response. The damping of the mea-

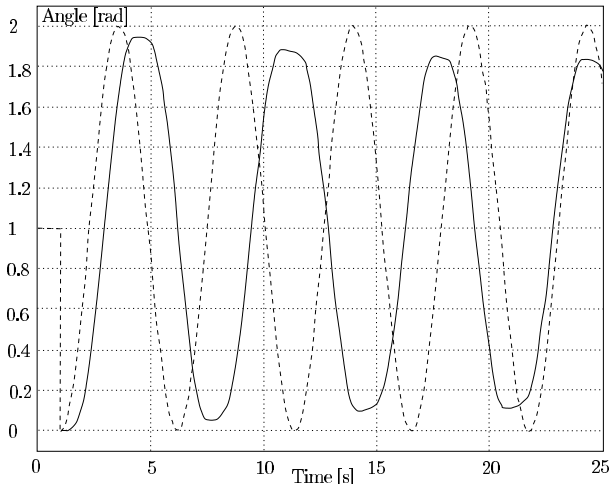

Fig. 5. LuGre model: – · –:desired angle; –:real motor; - -:ideal motor.

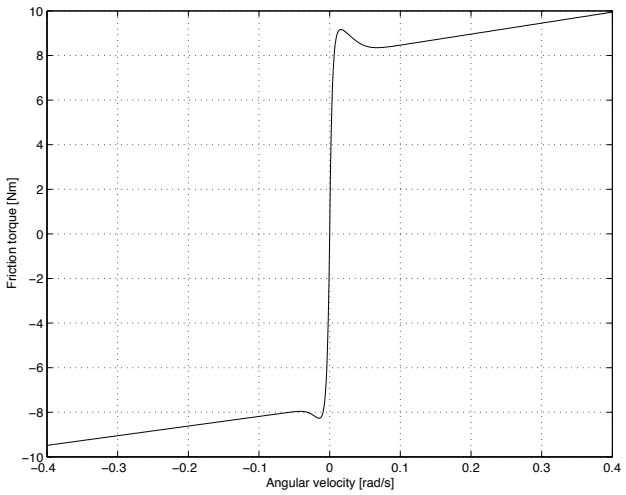

Fig. 6. Exponential friction compensation map.

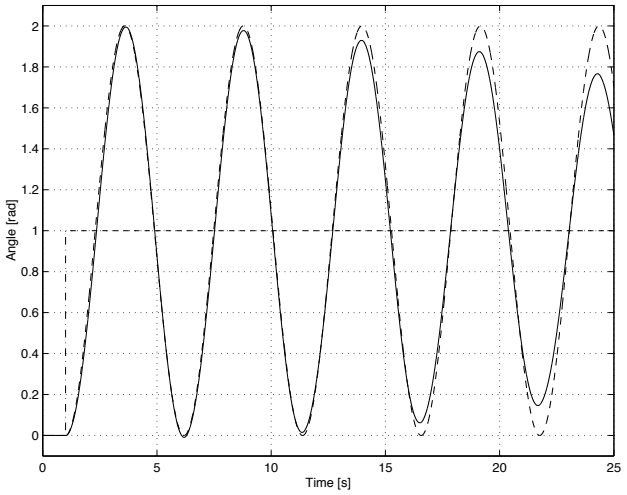

Fig. 7. Exponential friction compensation: – · – :desired angle; –:real motor; - -:ideal motor.

sured signal indicates the desired small under compensation of joint friction but the flattening of the response curve at its extrema shows that the motor is sticking at velocity reversals. This occurs because of an over estimate of the contribution of the dynamic friction contribution to the model[6]. The discrete nature of the system limits the range of possible dynamic parameters[6] and it was necessary to adopt the exponential friction model for use in the compensator.

B. Friction Compensation with the Exponential Model

The exponential friction compensation was chosen because the static parameters of the LuGre model had more influence on the estimated friction than the dynamic parameters and this friction compensation method is equivalent to the static part of the LuGre model, *i.e.* the static parameters of the LuGre model can be used for the exponential model.

A modification had to be made to the friction–velocity map: Since the map had an infinite slope at zero velocity, it was very sensitive to the smallest deformations of the motor and measurement noise. Therefore, the slope was decreased by multiplying each side of the map by

$$1 - \exp\left(-\left|\dot{\theta}\right| k_S\right) \tag{9}$$

where k_S is a factor used to adjust the slope (see Fig. 6). Decreasing the slope reduces the modelled stiction and therefore the performance of the friction compensation. A compromise between friction compensation performance and suppression of chattering was made to determine that $k_S = 300$ was the best choice. This model was validated in the same way as the LuGre model with the same P-gain value and 1 radian step input. The parameters for the modified friction compensation scheme were changed to $k_\gamma = 100$ s, $k_\tau = 1$ rad/Nms and $\delta = \pm 0.01$ s^{-1}. The step response is shown in Fig. 7 as a solid line; the dashed line denotes an ideal model. Very good agreement between the friction compensated actuator and an ideal motor model is given with this friction compensation. There is the desired under damping and no chattering or ripples.

To demonstrate the back drivability experimentally, a torque was applied to the motor shaft and the ensuing shaft motion was measured. The applied torque and shaft speed are plotted together in Fig. 8. As expected for an ideal system, a torque pulse leads to a change in velocity; if no torque is applied, the velocity stays constant. With the property that it is independent from the surrounding control algorithm, it fulfills all requirements of friction compensation.

V. PASSIVITY BASED CONTROL OF THE FLEXIBLE MANIPULATOR

The control of flexible robots is more complex than the control of rigid robots. The control objective in both cases is usually the positioning of the end-effector with respect to the base frame of the robot. This should be done as precisely as possible and often as fast as possible.

In the rigid case, a simple position or velocity control of the actuators satisfies the control objective, because it is assumed that there are no significant dynamics between the motor shaft and the behavior of the attached linkage.

In the flexible case, each arm is a part of the manipulator with very complex dynamics. It can experience several

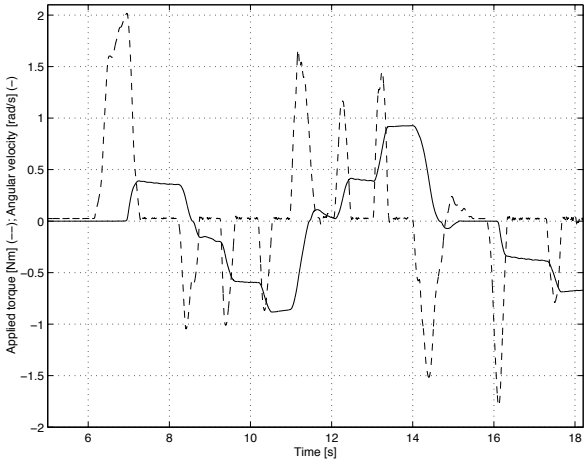

Fig. 8. Back drivability: -:angular velocity; - -:applied torque.

modes of oscillation and has solid friction components. The actuators themselves have joint flexibility due to their construction and, in the case of HD actuators, significant friction. To meet the control objective, these additional dynamic effects have to be taken into account.

A passivity based controller is often used for applications where no plant model exists or the model is inaccurate. It is based on the idea of extracting the kinetic energy from the system to stabilize it. The viewpoint moves away from the idea of a system with internal states to a device that interacts with its environment by transforming inputs to outputs. Input/output pairs are called *passive* when the system between them dissipates energy, *i.e.* it could be modelled analog to an electrical system containing only resistors, inductors, and capacitors. If such an input/output pair can be found for the system, the passivity theory says that any passive controller in a negative feed-back loop can stabilize the closed-loop system.

Damaren [9] has proven the passivity for a two link flexible manipulator using the passive input/output pair: actuator torques/cartesian endpoint rates. Based on this finding, a passive controller can stabilize the manipulator with simultaneous vibration suppression.

A PD-control law proposed by Damaren [9] to stabilize a flexible two link manipulator is

$$\tau = -\mathbf{J}_\theta^T[\mathbf{K}_d\dot{\rho}_\mu + \mathbf{K}_p(\rho_\mu - \rho_d)] \tag{10}$$

where τ is the vector of actuator torques, ρ_μ is the position vector of the end-effector in cartesian coordinates ($\dot{\rho}_\mu$ is its time derivative), ρ_d is the desired position in cartesian coordinates, $\mathbf{J}_\theta$ is the Jacobian of the rigid two link manipulator, and $\mathbf{K}_p, \mathbf{K}_d$ are the PD-gain matrices. The closed loop system can be expected to be stable for $\mathbf{K}_p = \mathbf{K}_p^T,\ \det(\mathbf{K}_p^T) > \mathbf{0}$ and $\mathbf{K}_d = \mathbf{K}_d^T,\ \det(\mathbf{K}_d^T) > \mathbf{0}$. The endpoint position ρ_μ is generated by

$$\rho_\mu = (1-\mu)\rho_r + \mu\rho_f \tag{11}$$

where ρ_r is the cartesian position assuming pure rigid links and ρ_f is the real end-effector position. The factor $0 < \mu < 1$ assures that the elastic coordinates stay observable – it should be chosen close but not equal to one.

The end-effector position ρ_f is determined by approximating the beam shape with a n^{th} order polynomial $w(x)$. Link 1 is equipped with three strain gage bridges; together with the the boundary conditions $w(0) = 0$ and $w'(0) = 0$ the five coefficients of a fourth order polynomial can be determined. Link 2 was approximated by a third order polynomial, because it has only two strain measurement locations.

Links $i = 1$ and $i = 2$ are approximated by

$$w_i(x_i) = b_{i0} + b_{i1}x_i + b_{i2}x_i^2 + b_{i3}x_i^3 + b_{i4}x_i^4 \tag{12}$$

The two boundary conditions lead to $b_{i0} = b_{i1} = 0$, $i \in \{1,2\}$. The strain at position x_i is approximated as

$$\varepsilon(x_i) = -t_1 w_i''(x_i)/2 = -t_1\left(b_{i2} + 3b_{i3}x_i + 6b_{i4}x_i^2\right) \tag{13}$$

where t_i denotes the thickness of link i. The coefficients can be determined by an on-line solution of

$$\begin{bmatrix} b_{i2} \\ b_{i3} \\ b_{i4} \end{bmatrix} = -\frac{2}{t_i}\begin{bmatrix} 2 & 6x_{iA} & 12x_{iA}^2 \\ 2 & 6x_{iB} & 12x_{iB}^2 \\ 2 & 6x_{iC} & 12x_{iC}^2 \end{bmatrix}^{-1}\begin{bmatrix} \varepsilon_A \\ \varepsilon_B \\ \varepsilon_C \end{bmatrix}. \tag{14}$$

With the coefficients calculated, the deflection v_i and the angle α_i of the end of the link is given by

$$v_i = b_2L_i^2 + b_3L_i^3 + b_4L_i^4 \qquad \alpha_i = v_i'(x_i)\big|_{x_i=L_1} \tag{15}$$

where L_i denotes the length of the flexible part of Link i.

Flexible forward kinematics were determined to map joint angles, link deflections, and link angles to cartesian coordinates. They were derived geometrically. Since the deformations were small compared to the length of the links, it was assumed that the length of each link from the root to the end stays constant.

$$\rho_\mu = \begin{bmatrix} x_f & y_f \end{bmatrix}^T \tag{16}$$

$$\begin{aligned} x_f = {} & (l_{1a}+l_{1b})\cos\theta_1 - v_1\sin\theta_1 + l_{1c}\cos(\theta_1+\alpha_1) \\ & +(l_{2a}+l_{2b})\cos(\theta_1+\alpha_1+\theta_2) - v_2\sin(\theta_1+\alpha_1+\theta_2) \\ & +l_{2c}\cos(\theta_1+\alpha_1+\theta_2+\alpha_2) \end{aligned} \tag{17}$$

$$\begin{aligned} y_f = {} & (l_{1a}+l_{1b})\sin\theta_1 + v_1\cos\theta_1 + l_{1c}\sin(\theta_1+\alpha_1) \\ & +(l_{2a}+l_{2b})\sin(\theta_1+\alpha_1+\theta_2) + v_2\cos(\theta_1+\alpha_1+\theta_2) \\ & +l_{2c}\sin(\theta_1+\alpha_1+\theta_2+\alpha_2) \end{aligned} \tag{18}$$

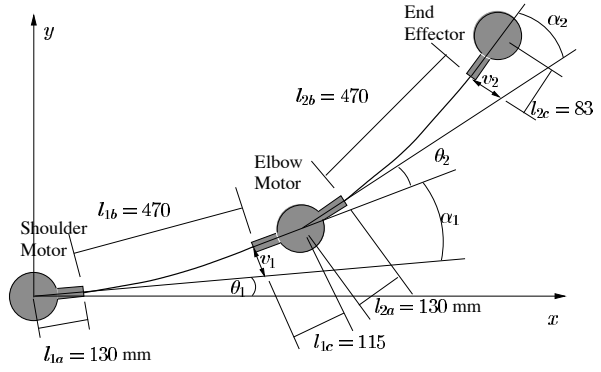

Fig. 9. Dimensions and variables of the manipulator (in *mm*).

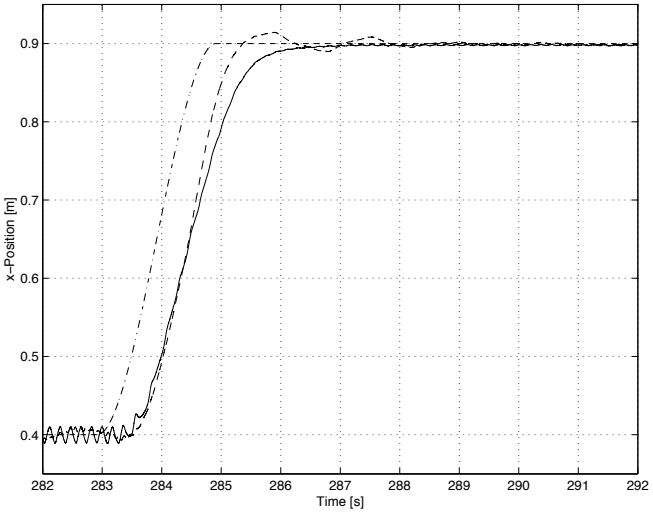

Fig. 10. Following x-trajectory: $-\cdot-$:desired position; –:flexible feed-back; - -:rigid feed-back.

l_{ik} denote the lengths shown in Fig. 9.

The control law (10) was implemented with the parameters

$$\mu = 0.6 \quad \mathbf{K}_p = \begin{bmatrix} 500 & 0 \\ 0 & 500 \end{bmatrix} \quad \mathbf{K}_d = \begin{bmatrix} 200 & 0 \\ 0 & 200 \end{bmatrix}.$$

To get reasonable derivatives the measured signals were filtered by a second order digital Butterworth filter: the angle filter had a cutoff frequency of $10Hz$, and the strain measurements filter had a cutoff frequency of $50Hz$.

The desired end-effector trajectory was designed to move the manipulator from rest to rest with the trajectory constraints $x_i(0) = 0,\ x_i'(0) = 0,\ x_i(T) = e,\ x_i'(T) = 0$, the trajectory for each coordinate x_i was a third order polynomial

$$x_i(t) = c_{i0} + c_{i1}t + c_{i2}t^2 + c_{i3}t^3 \tag{19}$$

$$c_{i0} = 0 \qquad c_{i1} = 0 \qquad c_{i2} = \frac{3e_i}{T^2} \quad c_{i3} = -\frac{2e_i}{T^3} \tag{20}$$

where e_i is the end-position of the trajectory and the duration $T = 3s$ was chosen for a movement from $[x = 1.1m, y = 0.4m]$ to $[0.5m, 0.9m]$. The results in cartesian coordinates are shown in Fig. 10 and 11. Two cases are shown in each figure: (1) The controller is using the flexible feed-back $\mu = 0.6$, (2) The controller is using the rigid feed-back $\mu = 0$.

A second experiment emphasizes the disturbance rejection of the controller (Fig. 12) where a force pulse was applied to the end-effector.

The controller is able to move the end-effector along a desired trajectory with only small oscillations. But when the end-effector is approaching the desired position, the controller introduces a fast oscillation with small magnitude. This oscillation likely arises from the delay caused by the derivation and by the filtering of the signals. The comparison to the rigid feed-back case shows, that this oscillation is introduced by the flexible feed-back signal. Since the motor torques are chattering with the frequency of the oscillation, this behavior is not desirable, and the oscillation should be reduced in further approaches. The reason for the tracking delay is the pure position control ($\dot{\rho}_d = \mathbf{0}$), *i.e.* providing the velocity trajectory in addition to the position trajectory will reduce this lag. The damping of disturbances is, as Fig. 12 shows, quite fast.

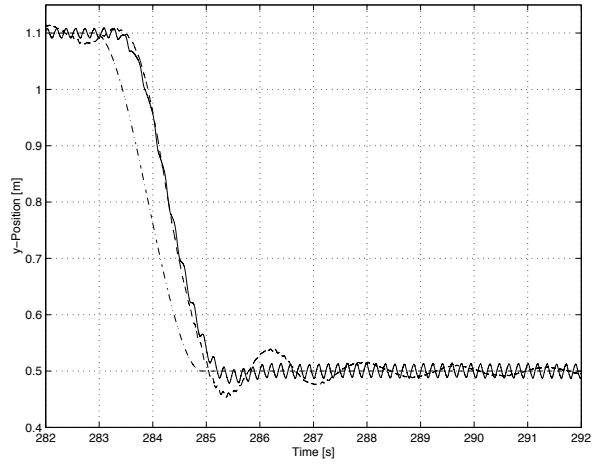

Fig. 11. Following y-trajectory: $-\cdot-$:desired position; –:flexible feed-back; - -:rigid feedback.

VI. SUMMARY

Experiments on HD actuators showed that static, compared to dynamic, friction effects are dominant and a static model was ultimately chosen for friction compensation. Because of the high static internal friction of the actuators, the modified friction compensation scheme was developed. The application of this simple effective friction compensation to the HD actuators removed the non-linear behavior almost completely and allows the successful application of a controller designed for use with more linear direct drive actuators.

REFERENCES

[1] Brian Armstrong-Hélouvry, Pierre Dupont, and Carlos Canudas de Wit. "A survey of models, analysis tools and compensation methods for the control of machines with friction", *Automatica*, vol. 30, no. 7, 1994, pp 1083–1138.

[2] H. Olsson, K. J. Åström, C. Canudas de Wit, M. Gäfvert, and P. Lischinsky. "Friction models and friction compensation", *European Journal of Control*, Dec. 1998, No.4, pp 176–195.

[3] R. Stribeck. "Die wesentlichen Eigenschaften der Gleit- und Rollenlager– The key qualities of sliding and roller bearings", *Zeitschrift des Vereines Deutscher Ingenieure*, vol. 46, no. 38,39, 1902, pp 1342–1348,1432–1437.

[4] C. Canudas de Wit, H. Olsson, K. J. Åström, and P. Lischinsky. "A new model for control of systems with friction", *IEEE Transactions on Automatic Control*, vol. 40, no. 3, March 1995, pp 419–425.

[5] Philip R. Dahl. "Solid friction damping of mechanical vibrations", *AIAA Journal*, vol. 14, no. 12, December 1976, pp 1675–1682.

[6] Jan-Peter Hauschild. "Control of a flexible link robotic manipulator in zero gravity conditions", Technical report, University of Waterloo, Ontario, Canada, August 2003.

[7] P. Shi, J. McPhee, and G. Heppler. "Design and control of an experimental facility for emulating space-based robotic manipulators", *in* 31^{ST} *International Symposium on Robotics*, Montreal, Canada, May 2000, pp 481–486.

[8] Magnus Gäfvert. "Comparisons of two dynamic friction models", *in Proc. 6th IEEE Conf. on Control Applications*, Hartford, CT, October 1997, pp 386–391.

[9] Christopher J. Damaren. Modal properties and control system design for two-link flexible manipulators. *International Journal of Robotics Research*, vol. 17, no. 6, June 1998, pp 667–678.

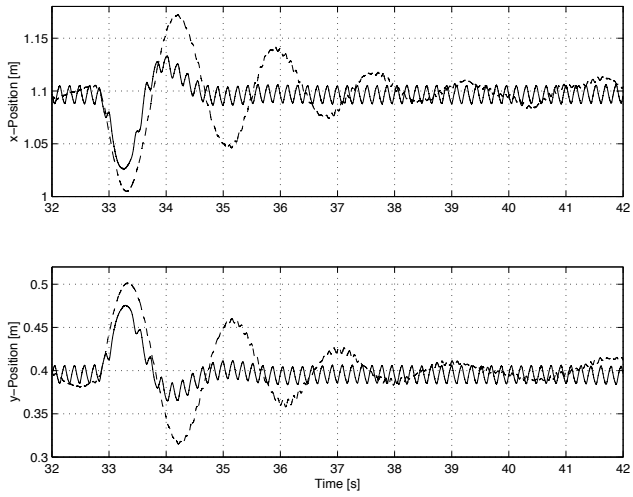

Fig. 12. Disturbance rejection: –:flexible feed-back; - -:rigid feed-back.